W- and X-Band Pulsed Electron Nuclear Double-Resonance Study of a Sodium−Nitric Oxide Adsorption Complex in NaA Zeolites

Andreas Pöppl,*,† Thomas Rudolf,† Palanichamy Manikandan,‡ and Daniella Goldfarb‡

Contribution from the Fakultät für Physik und Geowissenschaften, Universität Leipzig, Linnéstrasse 5, D-04103 Leipzig, Germany, and The Weizmann Institute of Science, Rehovot, Israel 76100

Received May 30, 2000

Abstract: Pulsed electron nuclear double-resonance (ENDOR) spectroscopy at W- and X-band frequencies has been employed to characterize the structure of NO adsorption sites involving sodium cations in zeolite NaA. The principal values of the sodium hyperfine and nuclear quadrupole coupling tensors as well as the orientation of their principal axes system with respect to the **g** tensor coordinate frame of the Na^+-NO adsorption complex could be determined by orientation-selective ENDOR spectroscopy. Such orientation-selective experiments benefit especially from the high spectral resolution at W-band frequencies. Furthermore, the sodium ENDOR spectrum is drastically simplified at high frequencies where the limit of weak hyperfine couplings is fulfilled. The dipolar sodium hyperfine coupling tensor reveals a bent structure of the formed adsorption complexes and gives access to the bond distance between the NO molecule and the cations. The ^{23}Na nuclear quadrupole data indicate that the adsorption complexes are preferentially formed with the sodium ions at the six-membered rings of the NaA zeolite structure. An analysis of the sodium and nitrogen hyperfine coupling data shows that 96% of the unpaired electron spin density in the Na^+-NO adsorption complex is localized in the nitrogen and oxygen $2p\pi$ orbitals of the NO ligand molecule.

1. Introduction

The study of the interaction of nitric oxide (NO) with metal ions is a major topic in coordination chemistry, catalysis, and biochemistry. In zeolite research, many investigations focus on the catalytic decomposition of NO into N_2 and O_2 over transition metal ion-exchanged zeolites.[1−4] The NO molecule has also attracted considerable interest since it can be used as a paramagnetic probe molecule to characterize the structure, concentration, and acid strength of Lewis acid sites on the basis of its unique chemical and spectroscopic properties.[5−11] Such Lewis acid sites in zeolites can be cations (M^{n+}) or aluminum defect centers $(Al_xO_y)^{n+}$, both of which form adsorption sites for NO molecules.

In gaseous NO, the $^2\Pi_{1/2}$ ground state of the molecule is diamagnetic as the spin and orbital angular momentum cancel each other.[12,13] However, upon adsorption, the orbital angular momentum is quenched by the electric fields at the adsorption site. The $^2\Pi_{1/2}$ ground state becomes paramagnetic[5] and accessible to electron spin resonance (ESR) spectroscopy. This quenching of the orbital angular momentum is accompanied by the lifting of the degeneracy between the antibonding $^2\Pi_x^*$ and $^2\Pi_y^*$ orbitals, where the unpaired electron resides in the latter.[7,13] The energy splitting Δ between the $^2\Pi_x^*$ and $^2\Pi_y^*$ orbitals is measured by the principal values of the NO **g** tensor and can be used to characterize the electric field at the adsorption site of the probe molecule.[5−7] Furthermore, ESR investigations of the adsorption−desorption behavior of the NO molecules allow the direct determination of the adsorption energies of the NO probe molecules at the Lewis acid sites. This approach has recently been demonstrated for a Na^+-NO adsorption complex in zeolite NaA[11] and has the potential to provide a unique site-specific tool for a direct quantitative measurement of the acid strength of the Lewis acid sites. However, the particular adsorption sites and the coordination geometry of the formed NO adsorption complexes are yet to be explored. Such information can be obtained from the hyperfine (hf) interaction between the unpaired electron spin at the NO molecules and the nuclear spin at the metal ions which form the Lewis acid sites. Unfortunately, metal ion hf couplings have only been resolved in continuous wave (cw) ESR spectra of a few NO adsorption complexes, including $(Al_xO_y)^{n+}-NO$[5,7,8,10] and Cu^+-NO.[14] In the case of Na^+-NO adsorption complexes, the spectral resolution of cw ESR experiments is not sufficient to resolve the sodium hf coupling.[6−8,11,15]

In this work we employ orientation-selective pulsed electron nuclear double-resonance (ENDOR) spectroscopy at W- and X-band frequencies to explore the coordination geometry of a Na^+-NO adsorption complex in zeolite NaA. The ESR powder

(1) Iwamoto, M.; Hamda, H. *Catal. Today* **1991**, *10,* 57.
(2) Centi, G.; Perathoner, S. *Appl. Catal. A: General* **1995**, *132,* 179.
(3) Shelef, M. *Chem. Rev.* **1995**, *95,* 209.
(4) Traa, Y.; Burger, B.; Weitkamp, J. *Microporous Mesoporous Mater.* **1999**, *30,* 3.
(5) Lundsford, J. H. *J. Phys. Chem.* **1968**, *72,* 4163.
(6) Hoffman, B. M.; Nelson, N. J. *J. Chem. Phys.* **1969**, *50,* 2598.
(7) Kasai, P. H.; Bishop, R. J., Jr. In *Zeolite Chemistry and Catalysis*; Rabo, J. A., Ed.; ACS Monograph 171; American Chemical Society: Washington, DC, 1976; pp 350−391.
(8) Gutsze, A.; Plato, M.; Karge, H. G.; Witzel, F. *J. Chem. Soc., Faraday Trans.* **1996**, *92,* 2495.
(9) Seidel, A.; Gutsze, A.; Boddenberg, B. *Chem. Phys. Lett.* **1997**, *275,* 113.
(10) Pöppl, A.; Rudolf, T.; Michel, D. *J. Am. Chem. Soc.* **1998**, *120,* 4879.
(11) Rudolf, T.; Pöppl, A.; Brunner, W.; Michel, D. *Magn. Reson. Chem.* **1999**, *37,* 93.
(12) Beringer, R.; Castle, J. G. *Phys. Rev.* **1950**, *78,* 581.
(13) Dousmanis, G. C. *Phys. Rev.* **1995**, *97,* 967.
(14) (a) Naccache, C.; Che, M.; Ben Taarit, Y. *Chem Phys. Lett.* **1972**, *13,* 109. (b) Lunsford, J. H.; Chao, C. C. *J. Phys. Chem.* **1972**, *76,* 1546. (c) Sojka, Z.; Che, M.; Giamello, E. *J. Phys. Chem.* **1997**, *101,* 4831.

10.1021/ja001888u CCC: $19.00
Published on Web 10/03/2000

spectrum of the Na^+-NO complex is governed by two strongly anisotropic interactions, the field-dependent electron Zeeman interaction and the field-independent ^{14}N hf coupling. The nitrogen hf coupling tensor $\mathbf{A}^N$, with its principal values $A_{xx}^N \approx 0$, $A_{yy}^N \approx 91$ MHz, and $A_{zz}^N \approx 0$ is axially symmetric within the accuracy of the ESR results, whereas the principal values of the electron **g** tensor, $g_{xx} = 1.999$, $g_{yy} = 1.993$, $g_{zz} = 1.884$, indicate an orthorhombic symmetry.[11,15] As the deviation of the **g** tensor from axial symmetry is small, the analysis of the orientation-selective ^{23}Na ENDOR experiments benefits especially from the high spectral resolution at W-band (94 GHz) frequencies since the g_{xx} spectral position can readily be distinguished from the g_{yy} region. This, in turn, allows us to unambiguously determine the principal values and the orientation of the principal axes of the sodium hf coupling tensor with respect to the *x* and *y* axes of the **g** tensor. The geometry of the Na^+-NO adsorption complex can then be deduced from these ^{23}Na hf coupling data. Orientation-selective ENDOR spectroscopy provides also the opportunity to determine the ^{14}N hf coupling along the *x* and *z* axes of the **g** tensor, which is too small to be resolved in cw ESR experiments.[11,15] From the nitrogen and sodium hf interactions, the spin densities in the molecular orbitals of the Na^+-NO complex can be derived to give insight into the electronic structure of the adsorption complex.

2. Simulation of Orientation-Selective ENDOR Spectra

The theory of orientation-selective ENDOR spectroscopy has already been discussed in a series of publications.[16−18] Therefore, we give only a brief outline of the simulation procedure used.

In the first step of the calculation, the **g** tensor orientations that contribute to the ESR resonance positions at the selected magnetic field $\mathbf{B}_0$ in the orientation-selective ENDOR experiment have to be determined. The **g** tensor orientations are defined by pairs (θ_i,ϕ_i) of horizontal and azimuthal angles θ and ϕ as usual. In the case of the Na^+-NO complex, the ESR powder pattern is governed by the anisotropic electron Zeeman and nitrogen hf interactions. The tensors of both interactions **g** and $\mathbf{A}^N$ are coaxial.[11,15] The ESR resonance positions at a given observer field B_0 in the ENDOR experiment are then expressed by the well-known relation[17]

$$B_0 = \frac{h\nu_{mw} - \sum_{i=1}^{3} A(\theta,\phi) m_i^N}{\beta_e g(\theta,\phi)} \qquad (1)$$

where ν_{mw} is the microwave (mw) frequency, $m_i^N = -1, 0, 1$ are the magnetic spin quantum numbers of the ^{14}N nuclei ($I = 1$), and all other symbols have their usual meaning. The effective *g* value and hf coupling *A* are given by

$$g(\theta,\phi) = \left(\sum_j g_{jj}^2 l_j^2\right)^{1/2}$$

$$A(\theta,\phi) = \left(\frac{\sum_j (A_{jj}^N g_j l_j)^2}{g(\theta,\phi)}\right)^{1/2}, \quad j = x, y, z \qquad (2)$$

with the direction cosines

$$l_x = \cos\phi \sin\theta, \quad l_y = \sin\phi \cos\theta, \quad l_x = \cos\theta \qquad (3)$$

defining the orientation of the external magnetic field $\mathbf{B}_0$ with respect to the **g** tensor frame. The selected orientations (θ_i,ϕ_i) at the observer field B_0 are then determined by calculating the ESR spectrum according to eqs 1−3 and searching for all the **g** tensor orientations that give rise to a resonance position within the field interval $B_0 \pm \Delta B_{12}^{inh}$. Here it is assumed that the bandwidth of the mw pulses in the pulsed ENDOR experiments is smaller than the inhomogeneous ESR line width ΔB_{12}^{inh} and can consequently be neglected.

The ENDOR spectra are calculated from the selected orientations (θ_i,ϕ_i) by an exact diagonalization of the spin Hamiltonian given in the **g** tensor principal axes system,[19]

$$\hat{H} = \beta_e B_0(0,0,1)\tilde{\mathbf{R}}(\phi_i,\theta_i,0)\mathbf{g}\hat{\mathbf{S}} - \beta_n g_l B_0(0,0,1)\tilde{\mathbf{R}}(\phi_i,\theta_i,0)\hat{\mathbf{I}}^1 + \hat{\mathbf{S}}\tilde{\mathbf{R}}(\alpha,\beta,\gamma)\mathbf{A}^1\mathbf{R}(\alpha,\beta,\gamma)\hat{\mathbf{I}}^1 + \hat{\mathbf{I}}^1\tilde{\mathbf{R}}(\alpha',\beta',\gamma')\mathbf{Q}^1\mathbf{R}(\alpha',\beta',\gamma')\hat{\mathbf{I}}^1 \qquad (4)$$

where g_l is the nuclear *g*-factor and $\mathbf{A}^1$ and $\mathbf{Q}^1$ are the hf and nuclear quadrupole (nq) interaction tensors of the ligand nucleus, both given in their principal coordinate system. The quantity **R** is the Euler matrix. The two sets of Euler angles α,β,γ and α',β',γ', define the transformation of the diagonal $\mathbf{A}^1$ and $\mathbf{Q}^1$ tensors into the **g** tensor coordinate frame. The ENDOR transition frequencies ν_{ij} are calculated from the differences between the obtained eigenvalues, $\nu_{ij} = (E_i - E_j)/h$, within the two electron spin manifolds $m_S = \pm^1/_2$. For each frequency ν_{ij}, the relative ENDOR intensities P_{ij} were obtained from the matrix elements,

$$P_{ij} = \langle\psi_i|B_{rf}(0,1,0)\tilde{\mathbf{R}}(\phi_i,\theta_i,0)(-\beta_n g_l \hat{\mathbf{I}}^1 + \beta_e \mathbf{g}\hat{\mathbf{S}})|\psi_j\rangle^2 \qquad (5)$$

where ψ_i and ψ_j are the corresponding eigenvectors of the spin states *i* and *j*. Equation 5 takes into account the interaction between the radio frequency field B_{rf} and the electron spin that gives rise to the so-called hyperfine enhancement.[19] This interaction may lead to pronounced differences in the ENDOR intensities between signals from different m_S states in experiments at conventional mw frequencies such as in X-band measurements.[20] However, also at the W-band, the hyperfine enhancement effect cannot be neglected, as shown below. For the simulation of the orientation-selective ENDOR spectra, the above procedure is repeated for each set of contributing **g** tensor orientations (θ_i,ϕ_i). The final ENDOR spectrum is then obtained by adding all individual ENDOR spectra using a Gaussian weighting function with a variance ΔB_{12}^{inh}.

3. Experimental Section

Sample Preparation. The NaA zeolite was synthesized according to standard procedures.[21] The zeolite material was activated by dehydration at $T = 750$ K in a stainless steel vacuum line at a pressure of 10^{-7} mbar for 24 h and subsequently treated with 200 mbar of oxygen at the same temperature for 1 h to remove residual organic impurities. The samples were then evacuated again to a pressure of about 10^{-6} mbar. Nitric oxide was adsorbed onto activated NaA samples at room temperature with a gas pressure corresponding to approximately 10^{-2} molecules per unit cell. The sample preparation was carefully checked

(15) Biglino, D.; Li, H.; Erickson, R.; Lund, A.; Yahiro, H.; Shiotani, M. *Phys. Chem. Chem. Phys.* **1999**, *1*, 2887.
(16) Hoffman, B. M.; Martinsen, J.; Venters, R. A. *J. Magn. Reson.* **1984**, *59*, 110.
(17) Hurst, G. C.; Henderson, T. A.; Kreilick, R. W. *J. Am. Chem. Soc.* **1985**, *107*, 7294.
(18) Kreiter, A.; Hüttermann, J. *J. Magn. Reson.* **1991**, *93*, 12.
(19) Schweiger, A.; Günthard, Hs. H. *Chem. Phys.* **1982**, *70*, 1.
(20) Schweiger, A. *Structure and Bonding*; Springer: Berlin, 1982; Vol. 51.
(21) Thompson, R. W.; Huber, M. J. *J. Cryst. Growth* **1982**, *56*, 711.

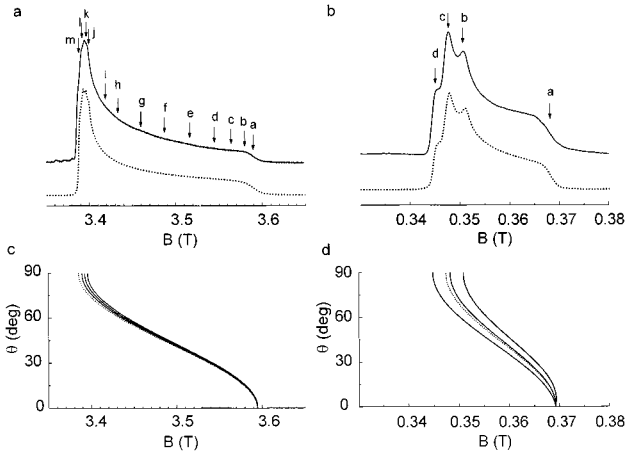

Figure 1. W- and X-band two-pulse field swept ESE spectrum of the Na^+-NO adsorption complex in zeolite NaA: experimental (solid line) and simulated (dashed line) (a) W- and (b) X-band spectra. Calculated magnetic resonance fields in the **g** tensor *xz* (dashed line) and *yz* (solid lines) plane at (c) W- and (d) X-band. Simulation parameters are given in the text.

by the observation of the well-known nine-line ESR signal of the paramagnetic $^2\Pi_{3/2}$ state of gaseous nitric oxide at room temperature.[11,12]

Spectroscopic Measurements. Pulsed ENDOR and two-pulse field-swept electron spin−echo (ESE) experiments at the W-band were carried out at $T = 4.3$ K with a mw frequency $\nu_{mw} = 94.9$ GHz on a home-built spectrometer described elsewhere.[22] X-band experiments were performed at $T = 5$ K with $\nu_{mw} = 9.68$ GHz on a Bruker ESP 380 spectrometer. For the two-pulse field-swept ESE measurements, mw pulse lengths of $t_{\pi/2} = 50$ ns for $\pi/2$ pulses and $t_\pi = 100$ ns for π pulses with a pulse delay of $\tau = 300$ ns (W-band) and $t_{\pi/2} = 100$ ns, $t_\pi = 200$ ns, $\tau = 1.4$ μs (X-band) were used. Both the Davies[23] and the Mims[24] ENDOR sequences were employed in the W-band experiments, whereas only the Davies ENDOR sequence was used at X-band frequencies. Mims ENDOR experiments were carried out with $t_{\pi/2} =$ 120 ns, $\tau = 250$ ns, and a radio frequency pulse width of $t_{rf} = 12$ μs. Pulse lengths and delays of $t_{\pi/2} = 100$ ns, $t_\pi = 200$ ns, $t_{rf} = 12$ μs, τ $= 400$ ns (W-band) and $t_{\pi/2} = 200$ ns, $t_\pi = 400$ ns, $t_{rf} = 10$ μs, $\tau = 1.2$ μs (X-band) were applied in measurements using the Davies ENDOR sequence.

4. Results

Field-Swept ESE. Two-pulse field-swept ESE spectra of the Na^+-NO adsorption complex in zeolite NaA were taken at W- and X-band frequencies. The experimental spectra are illustrated in Figure 1a,b. Both spectra reveal substantial anisotropic electron Zeeman and nitrogen hf interactions. Simulations of the experimental spectra were obtained using second-order perturbation theory with an orthorhombic **g** tensor with $g_{xx} =$ 2.001, $g_{yy} = 1.996$, $g_{zz} = 1.888$ and an axially symmetric nitrogen hf coupling tensor with $A^N_{xx} \approx A^N_{zz} \approx 0$, $A^N_{yy} \approx 91$ MHz, in good agreement with previously published results.[11,15] The calculation of the ESR resonance fields in the **g** tensor *xz* and *xy* planes as a function of the angle θ between the external magnetic field and the *z* axis of the **g** tensor is useful for the selection of proper field positions for the orientation-selective ENDOR measurements. Such θ versus resonance field plots, calculated from the estimated principal values of the **g** and $\mathbf{A^N}$ tensors of the Na^+-NO complex according to eq 1, are presented in Figure 1c,d.

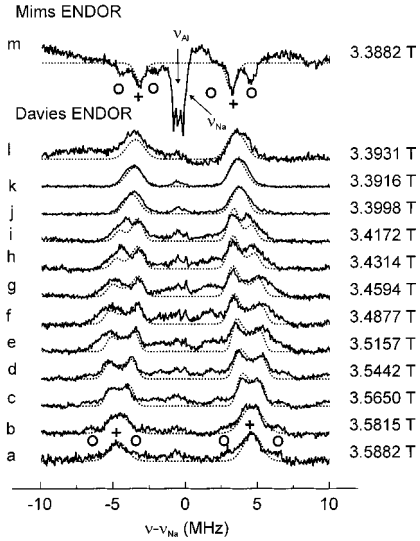

Figure 2. Experimental (solid lines) and simulated (dashed lines) W-band orientation-selective Davies (a−l) and Mims (m) ENDOR spectra of the Na^+-NO adsorption complex in zeolite NaA. ν_{Na} and ν_{Al} indicate the free ^{23}Na and ^{27}Al nuclear Larmor frequencies in the Mims ENDOR spectrum (m). The simulations took into account only the ^{23}Na hf coupling, and the ^{23}Na nq interaction was neglected. Crosses and circles mark $m_I = {}^1/_2 \leftrightarrow -{}^1/_2$ and $m_I = \pm{}^1/_2 \leftrightarrow \pm{}^3/_2$ ^{23}Na ENDOR transitions, respectively.

^{23}Na ENDOR. A series of orientation-selective W-band pulsed ENDOR spectra of the Na^+-NO adsorption complex in zeolite NaA is illustrated in Figure 2. The various magnetic field positions where the ENDOR spectra were taken are indicated by arrows in Figure 1a. All spectra reveal two groups of signals which are symmetrically situated with respect to the sodium nuclear Larmor frequency ν_{Na}. Therefore, they are assigned to ^{23}Na ENDOR transitions of the sodium ligand nucleus in the Na^+-NO complex belonging to two different m_S states (weak coupling case, $2\nu_{Na} > A^{Na}$). Furthermore, the Mims ENDOR spectrum (Figure 2m) displays an intense triplet with a total splitting of about 0.74 MHz, which is shifted by about 0.57 MHz from $\nu_{Na} = 38.13$ MHz toward lower frequencies. These lines can be assigned to signals from two groups of weakly coupled aluminum nuclei. A weak shoulder at the high-frequency side of the ^{27}Al triplet situated exactly at ν_{Na} indicates an additional signal from distant Na^+ cations. Such weak signals at the ^{23}Na Larmor frequency can also be observed in the Davies ENDOR spectra at different field settings (Figure 2a−l), although the ^{27}Al signals at ν_{Al} are strongly suppressed in those spectra.

The two ^{23}Na ENDOR signals have an average splitting of about 6−9 MHz, indicating a substantial isotropic sodium hf coupling. The observed additional splitting of each signal into two lines at intermediate field positions (Figure 2c−i) is typical for orientation-selective ENDOR spectra, where the ligand nuclei hf coupling tensor is not coaxial to the **g** tensor frame.[25] The high-frequency ENDOR components are always slightly more intense than those at low frequency. This is a manifestation of the hyperfine enhancement effect.[20] In the spectra recorded near the g_{zz} spectral region of the ESR powder pattern (Figure 2a−d), additional shoulders have been observed at each sodium ENDOR line. We assume that these shoulders are caused by the nq interaction of the ^{23}Na nucleus having a nuclear spin $I = {}^3/_2$. This interpretation is supported by the splitting of the sodium ENDOR signals into three lines observed for the

(22) Gromov, I.; Krymov, V.; Manikandan, P.; Arieli, D.; Goldfarb, D. *J. Magn. Reson.* **1999**, *139*, 78.
(23) Davies, E. R. *Phys. Lett. A* **1974**, *47A*, 1.
(24) Mims, W. B. *Proc. R. Soc. London* **1965**, *283*, 452.
(25) Atherton, N. M. *Priniciples of Electron Spin Resonance*; Prentice Hall: New York, 1993.

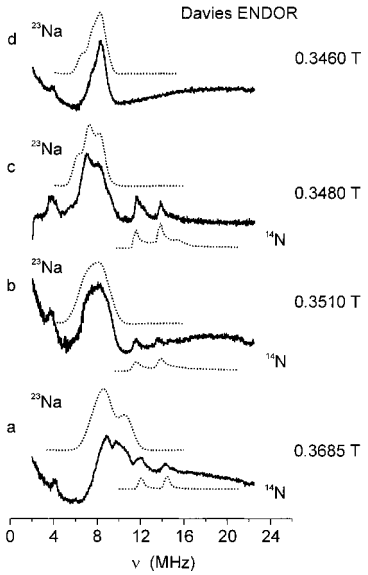

Figure 3. Experimental (solid lines) and simulated (dashed lines) X-band orientation-selective Davies ENDOR spectra of the Na^+-NO adsorption complex in zeolite NaA. The simulated ^{23}Na spectra were obtained from calculations where the hf and nq coupling was taken into account, whereas the ^{14}N spectra were computed without nq interaction.

spectrum taken at the single crystal-type g_{xx} position at the low-field edge of the ESR powder spectrum in Figure 2m, although baseline distortions somewhat obscure the nq triplets.

Orientation-selective X-band ENDOR spectra show only ^{23}Na ENDOR signals from one m_S state in the frequency range between 7 and 10 MHz (Figure 3). The ^{23}Na ENDOR signals from the second m_S state are expected to appear at frequencies below 2 MHz (intermediate coupling case, $2\nu_{Na} \approx A^{Na}$), a spectral range which is not accessible to our experimental setup. The two weak signals at about 12 and 14 MHz in Figure 3a−c are due to the nitrogen central nucleus hf interaction in Na^+-NO complex as discussed below. The ENDOR signal at about 4 MHz is assigned to weakly coupled distant ^{27}Al and ^{23}Na nuclei.

In the first step of the analysis of the ^{23}Na ligand ENDOR signals, only the ^{23}Na hf coupling was taken into account. Figure 2 shows that the maximum hf coupling of about $A^{Na} = 11$ MHz is observed in the ENDOR spectra d, e, and f, where intermediate **g** tensor orientations with $\theta \approx 25-45°$ are selected (Figure 1). The minimum hf coupling of approximately $A^{Na} = 6.3$ MHz is obtained from the central lines of the nq triplets in the spectrum taken at the g_{xx} spectral position ($\theta = 90°$) (Figure 2m). At this field position, **g** tensor orientations contribute only to the ENDOR spectrum, where the magnetic field points along the *x* axis of the **g** tensor frame. The hf coupling is slightly larger ($A^{Na} = 7.1$ MHz) in the spectra in Figure 3j−l, where orientations with **B** directed along the **g** tensor *y* axis are selected. However, other orientations within and close to the **g** tensor *xy* plane contribute also to those spectra, preventing an exact determination of the sodium hf coupling along the *y* axis of **g** from the W-band ENDOR spectra. But in an X-band experiment the g_{yy} position can readily be separated from other **g** tensor orientations by selecting the low-field edge of the ESR powder pattern (position d in Figure 1b). This ENDOR spectrum shows only a single ^{23}Na signal from one m_S state at about 8.0 MHz (Figure 3d) corresponding to about $A^{Na} = 8.1$ MHz. It seems to be noteworthy that an additional intense ^{23}Na signal appears at about 7.1 MHz in the ENDOR spectrum in Figure 3c, where spectral components at both positions, g_{yy} and g_{xx},

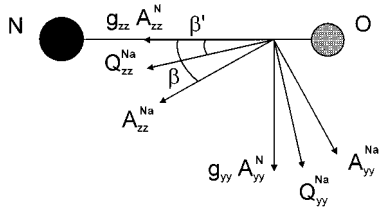

Figure 4. Deduced orientation of the principal axes systems of the **g**, $\mathbf{A}^N$, $\mathbf{A}^{Na}$, and $\mathbf{Q}^{Na}$ tensors of the Na^+-NO adsorption complexes. Note that the unpaired electron occupies a $^2\Pi^*_y$ orbital which points along the g_{yy} and A^N_{yy} principal axes. The A^N_{yy} direction is defined by the maximum ^{14}N hf coupling, which has already been resolved in the ESR experiment.

contribute to the ENDOR spectrum (Figure 1). This signal provides $A^{Na} = 6.3$ MHz, in good accordance with the sodium hf coupling determined for the g_{xx} position in the W-band experiments. The results are characteristic of an approximately axially symmetric hf interaction tensor whose *z* axis (principal axis corresponding to the largest principal value of the hf tensor) is lying within the **g** tensor *yz* plane and forms an angle with the g_{zz} direction of about 35°. Simulations of the W-band data with $A^{Na}_{xx} = A^{Na}_{yy} = 6.3 \pm 0.2$ MHz, $A^{Na}_{zz} = 10.9 \pm 0.2$ MHz, $\alpha = 90° \pm 5°$, $\beta = 35° \pm 5°$ agree with the experimental data well (Figure 2). Even the small differences in the intensities of the ENDOR signals from different m_S states due to the hyperfine enhancement are reproduced in the simulated spectra. The axial symmetry of the $\mathbf{A}^{Na}$ tensor together with the relations $A^{Na}_{zz} > A^{Na}_{xx,yy}$ implies that the sign of the principal values is positive. Note that the sodium nq coupling has not been taken into account in the simulations at this point. The simulations show that small changes in the deduced orientation of the ^{23}Na hf coupling tensor $\mathbf{A}^{Na}$ or small deviations from axial symmetry lead to significant shifts and an additional splitting of the simulated ^{23}Na ENDOR spectra. Therefore, the obtained parameter set seems to be unequivocal. The determined orientation of the principal axes system of ^{23}Na hf coupling tensor $\mathbf{A}^{Na}$ in the Na^+-NO complex with respect to the **g** tensor frame is schematically depicted in Figure 4.

In the second step we analyzed the sodium nq interaction. We start with the W-band spectra recorded at the g_{zz} and g_{xx} positions (Figure 2a and m), where the nq splittings are resolved. For both single-crystal-like positions we expect a theoretical intensity ratio between the two outer ^{23}Na ENDOR transitions ($m_I = \pm 1/2 \leftrightarrow \pm 3/2$) and the central $m_I = 1/2 \leftrightarrow -1/2$ transition of 3:4:3. The g_{xx} spectrum in Figure 2m resembles this intensity ratio, whereas in the spectrum taken at the g_{zz} position the outer $m_I = \pm 1/2 \leftrightarrow \pm 3/2$ transitions are considerably broadened in comparison with the central $m_I = 1/2 \leftrightarrow -1/2$ transitions and appear only as broad shoulders in the spectra in Figure 2a−d. This indicates a substantial distribution of the nq coupling for orientations close to the g_{zz} axis. A maximum ^{23}Na nq frequency of $\nu_Q \approx 1.92$ MHz is determined from the outer end positions of these shoulders of the ^{23}Na ENDOR signals in Figure 2c,d. This implies that the *z* axis (principal axis corresponding to the largest principal value) of the ^{23}Na nq coupling tensor $\mathbf{Q}^{Na}$ lies close to the *z* principal axis of the $\mathbf{A}^{Na}$ tensor. In the spectrum taken at the g_{xx} position (Figure 2m), a smaller nq frequency $\nu_Q \approx 1.23$ MHz is estimated from the triplet splitting of the ^{23}Na ENDOR signals. Quadrupole splittings are not detected in the ENDOR spectra where orientations along the **g** tensor *y* axis are selected (Figure 2j−l). On the basis of the line width of the ^{23}Na signals in these spectra, we conclude $\nu_Q < 0.69$ MHz for those orientations. The observed nq spitting suggests that the $\mathbf{Q}^{Na}$ tensor seems to be almost coaxial to the $\mathbf{A}^{Na}$ tensor

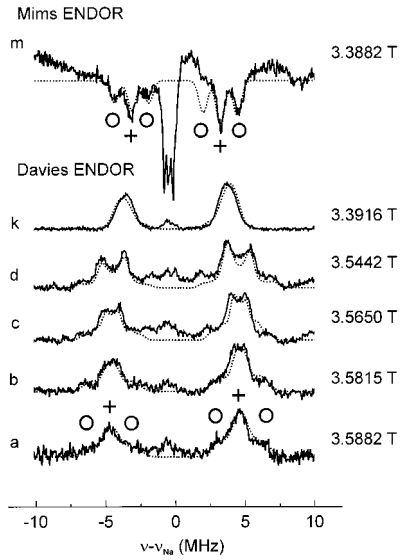

Figure 5. Some selected experimental (solid lines) and simulated (dashed lines) W-band orientation-selective Davies (a−d, k) and Mims (m) ENDOR spectra of the Na^+−NO adsorption complex in zeolite NaA, demonstrating the ^{23}Na nq effects. Crosses and circles mark $m_I = {}^1/_2 \leftrightarrow -{}^1/_2$ and $m_I = \pm{}^1/_2 \leftrightarrow \pm{}^3/_2$ ^{23}Na ENDOR transitions, respectively. In the simulations, both the ^{23}Na hf and nq interactions were taken into account.

($\alpha' \approx 90°$, $\beta' \approx 30°$, $\gamma' \approx -90°$), with principal values of about $|Q_{xx}^{Na}| = 0.41 \pm 0.03$ MHz, $|Q_{yy}^{Na}| \leq 0.23$ MHz, and $|Q_{zz}^{Na}| \leq 0.64$ MHz. The orientation of the principal axes of the $\mathbf{Q}^{Na}$ tensor with respect to the **g** tensor frame is likewise depicted in Figure 4. The broadening of the $m_I = \pm{}^1/_2 \leftrightarrow \pm{}^3/_2$ transitions in spectra where orientations close to the *z* principal axes of the $\mathbf{Q}^{Na}$ and $\mathbf{A}^{Na}$ tensors are selected (Figure 2a−d) and the relatively sharp $m_I = \pm{}^1/_2 \leftrightarrow \pm{}^3/_2$ transitions for orientations of the magnetic field along the $\mathbf{Q}^{Na}$ and $\mathbf{A}^{Na}$ tensor *x* axes (Figure 2m) indicate a substantial distribution in the Q_{zz}^{Na} and Q_{yy}^{Na} principal values as well as in the angle β'. Therefore, the determined nq parameters can only be regarded as rough estimates. The above suppositions are justified by further spectral simulations of some selected ^{23}Na W- and X-band ENDOR spectra, where the nq interaction was included in the calculations. In the simulations, variances in both the Euler angle $\beta' \approx 35° \pm 15°$ and the principal values $Q_{zz}^{Na} = 0.48 \pm 0.16$ MHz, $Q_{yy}^{Na} = -0.07 \pm 0.16$ MHz were assumed. Furthermore, the correlation among the nq principal values ($\sum Q_{ii}^{Na} = 0$) was taken into account. The other simulation parameters were $A_{xx}^{Na} = A_{yy}^{Na} = 6.3$ MHz, $A_{zz}^{Na} = 10.9$ MHz, $\alpha = 90°$, $\beta = 35°$, $Q_{xx}^{Na} = -0.41$ MHz, $\alpha' \approx 90°$, and $\gamma' \approx -90°$. The simulated X- and W-band ^{23}Na ENDOR spectra together with the experimental ones are depicted in Figures 3 and 5, respectively. All simulated spectra agree reasonably well with the experimental traces, considering the signal-to-noise ratio.

^{14}N ENDOR. In the ESR spectra of the Na^+−NO complex, a nitrogen hyperfine splitting with $A_{yy}^N \approx 91$ MHz can only be detected along the g_{yy} axis. Therefore, ^{14}N ENDOR spectroscopy has to be employed to determine the A_{xx}^N and A_{zz}^N principal values of the ^{14}N hf coupling tensor. In the X-band ENDOR spectra in Figure 3a−c two more weak signals at about 12 and 14 MHz can be observed besides the ^{23}Na signals. On the basis of the frequency spacing of these signals of about 2 MHz, they are assigned to ^{14}N hf interactions of the unpaired electron with the nitrogen nucleus in the Na^+−NO adsorption complex. No nitrogen signals could be detected in this frequency range in the ENDOR spectrum taken at the low-field edge of the ESR pattern (Figure 3d) corresponding to the g_{yy} position. This direction gives rise to the maximum nitrogen hf coupling ($A_{yy}^N \approx 91$ MHz) that is already resolved in the ESR spectrum (Figure 1). Consequently, a broad ENDOR signal (not shown) could only be detected at higher frequencies, $\nu \cong 40$ MHz, for the g_{yy} position. Otherwise, well-resolved ^{14}N ENDOR signals below 15 MHz can be observed at field positions for which orientations parallel to the *x* and *z* axes of the **g** and $\mathbf{A}^N$ tensors contribute to the ENDOR spectra (Figure 3a−c). For these orientations, the ESR spectra do not give any indication of a nitrogen hf splitting. If we assume coaxial $\mathbf{A}^N$ and **g** tensor principal axes systems,[7] as generally accepted for NO adsorption complexes, we may determine the principal values $A_{xx}^N = 25.3 \pm 0.2$ MHz and $A_{zz}^N = 26.3 \pm 0.2$ MHz of the nitrogen hf coupling tensor from the center of gravity (strong coupling case, $2\nu_N < A_{xx,zz}^N$) of the two ^{14}N ENDOR signals in Figure 3a,c. The ESR results provide the third principal value of the $\mathbf{A}^N$ tensor $A_{yy}^N = 91 \pm 5$ MHz.[11,15] Spectral simulations using the derived nitrogen hf coupling parameters are in good accordance with the experimental ENDOR spectra in Figure 3. Note that if A_{yy}^N is assumed to be positive, A_{xx}^N and A_{zz}^N must have likewise a positive sign to reproduce the asymmetric line shapes of the ^{14}N ENDOR signals in Figure 3.

5. Discussion

The determination of the sodium and nitrogen hf coupling tensors of the Na^+−NO adsorption complex in zeolite NaA by combined pulsed ENDOR experiments at W- and X-band frequencies allows us to characterize the complex structure in detail and to draw some general conclusions about the influence of the Na^+ cation adsorption site on the distribution of the valence electrons in the molecular orbitals of the adsorbed NO molecules. Furthermore, the ^{23}Na ENDOR spectra provided a rough estimate of the sodium nq coupling parameters, which opens some insight into the specific location of the NO adsorption site within the cavities of the zeolite.

Spin Density Distribution within the Na^+−NO Complex. From the principal values of the sodium hf interaction tensor, we determine an isotropic hf coupling $A_{iso}^{Na} = 7.8$ MHz. This translates into an unpaired electron spin density in the Na 3s orbital of $\rho_{3s}^{Na} = 0.9\%$.[26] The axial symmetry of the $\mathbf{A}^{Na}$ tensor implies that spin density contributions in sodium 3p orbitals are negligible. Therefore, the unpaired electron in the adsorption complex is mainly localized at the NO molecule.

The estimated ^{14}N hf interaction tensor $\mathbf{A}^N$ provides $A_{iso}^N = 47.7$ MHz and the principal values $B_{xx}^N = -22.4$ MHz, $B_{yy}^N = 43.8$ MHz, $B_{zz}^N = -21.4$ MHz of the dipolar nitrogen hf coupling tensor $\mathbf{B}^N$. The value A_{iso}^{Na} leads to a spin density of $\rho_{2s}^N = 3.1\%$ in the nitrogen 2s orbital.[26] The quantity ρ_{2s}^N must be considered as an upper limit for the unpaired spin density in the N 2s orbital since spin polarization in the 1s and 2s nitrogen orbitals cannot be neglected for NO groups.[27] From the dipolar nitrogen hf coupling calculated from the average of B_{xx}^N and B_{zz}^N, we deduce the spin density $\rho_{2p\pi}^N = 45.8\%$ in the N 2pπ orbital[26] that forms, together with the oxygen 2pπ orbital, the antibonding $^2\Pi_y^*$ molecular orbital, where the unpaired electron resides in the free NO molecule.[13] That leaves about $\rho_{2p\pi}^O = 50.2\%$ of spin density in the oxygen 2pπ orbital since

(26) Morton, J. R.; Preston, K. F. *J. Magn. Reson.* **1978**, *30*, 577.
(27) Cohen, A. H.; Hoffman, B. M. *J. Am. Chem. Soc.* **1973**, *95*, 2061.

$\rho_{total} = \rho_{3s}^{Na} + \rho_{2s}^{N} + \rho_{2p\pi}^{N} + \rho_{2p\pi}^{O}$. The wave function for the unpaired electron in the Na^+-NO complex is then given by

$$\psi = (0.46)^{1/2}\psi_{2p\pi}(N) + (0.03)^{1/2}\psi_{2s}(N) + (0.50)^{1/2}\psi_{2p\pi}(O) + (0.01)^{1/2}\psi_{3s}(Na) \quad (6)$$

The spin density distribution gives information about the change in the electronic structure of the NO molecule upon adsorption at the cation. It has been proposed that the electronic structure of NO is composed of a mixture of two resonance structures,[13]

$$\underset{\text{I}}{:\dot{N}=\ddot{O}:} \leftrightarrow \underset{\text{II}}{:\ddot{N}^{-}=\dot{O}:^{+}}$$

The unpaired spin densities $\rho_{2p\pi}^{N}$ and $\rho_{2p\pi}^{O}$ measure the contributions of structures I and II, respectively. If we compare the $\rho_{2p\pi}^{N}$ and $\rho_{2p\pi}^{O}$ values of the Na^+-NO adsorption complex with those obtained for free NO molecules,[13] $\rho_{2p\pi}^{N} = 0.65\%$, $\rho_{2p\pi}^{O} = 0.35\%$, we recognize an enhanced contribution of structure II to the total electronic structure of the NO molecule in the adsorption complex indicated by a shift of the unpaired spin density in the $^2\Pi_y^*$ molecular orbital toward the oxygen atom. This shift is caused by the electron pair acceptor property (Lewis acidity) of the sodium cation resulting in a net negative charge at the nitrogen atom in the adsorption complex,

$$Na^{+}-:\ddot{N}^{-}=\dot{O}:^{+}$$

The proposed electronic structure of the NO molecule in the adsorption complex indicates a substantial ionic bond contribution to the metal ion−NO bond and is supported by the small unpaired spin density at the sodium ion. Covalent bond contributions are expected to be small, which implies a weak bonding of the NO to the Na^+ cation. Actually, the adsorption complex is not thermally stable, as the desorption of the NO molexules from the cations starts at temperatures as low as 150 K.[11]

Coordination Geometry of the Na^+-NO Complex. The structure of the Na^+-NO complex can be deduced from the principal values and the orientation of the Na hf coupling tensor with respect to the coordinate frame of the **g** and $\mathbf{A}^N$ tensors. From $\mathbf{A}^{Na}$ and A_{iso}^{N}, the principal values of the dipolar sodium hf coupling tensor $\mathbf{B}^{Na}$ are determined to be $B_{xx}^{Na} = B_{yy}^{Na} = -1.55$ MHz and $B_{zz}^{Na} = 3.10$ MHz, where the angle between the *z* principal axes of the $\mathbf{B}^{Na}$ and **g** tensors is $\beta = 35°$ and B_{zz}^{Na} lies within the **g** tensor *yz* plane (Figure 4). Note that the *z* axis of the **g** tensor is aligned parallel to the N−O bond direction and the *y* axes of **g** and $\mathbf{A}^N$ tensors point along the symmetry axis of the $^2\Pi_y^*$ molecular orbital,[7] which lies within the Na^+-NO complex plane. The determined small spin density at the sodium ion justifies deriving the complex geometry from the dipolar Na hf coupling tensor within the framework of the dipole−dipole approximation. In this model, the interactions of the ^{23}Na nuclear spin with both the electron spin densities $\rho_{2p\pi}^{N}$ and $\rho_{2p\pi}^{O}$ in nitrogen and the oxygen $2p\pi$ orbitals must be taken into account. They give rise to two dipolar hf coupling tensors which can be calculated in the **g** tensor frame according to Hutchinson and McCay[28] by

$$\mathbf{B}_{K-Na}^{Na} = \frac{\beta_e\beta_n g_{Na}\rho_{2p\pi}^{K}}{r_{K-Na}^{3}} \times \begin{pmatrix} -g_{xx} & 0 & 0 \\ 0 & g_{yy}(3\sin^2\alpha_K - 1) & 3g_{yy}\sin\alpha_K\cos\alpha_K \\ 0 & 3g_{yy}\sin\alpha_K\cos\alpha_K & g_{zz}(3\cos^2\alpha_K - 1) \end{pmatrix}, \quad K = N, O \quad (7)$$

Here, r_{K-Na} is the distance between the Na^+ ion and the nitrogen or oxygen atom. The vector $\vec{r}_{K-Na}$, pointing from the N or O atom of the NO molecule to the cation, is assumed to be within the **g** tensor *yz* plane and forms an angle α_K with the g_{zz} axis. In this structural model, the quantities r_{O-Na} and α_O are given by

$$r_{O-Na} = \sqrt{2r_{NO}r_{N-Na}\cos\alpha_N + r_{NO}^2 + r_{N-Na}^2} \quad (8)$$

and

$$\cos\alpha_N = \frac{r_{N-Na}\cos\alpha_N + r_{NO}}{\sqrt{2r_{NO}r_{N-Na}\cos\alpha_N + r_{NO}^2 + r_{N-Na}^2}} \quad (9)$$

where $r_{NO} = 0.115$ nm is the bond length of the NO molecule.[29] The angle α_N is determined by the bond angle β_{bond} of the Na^+-NO complex,

$$\alpha_N = 180° - \beta_{bond} \quad (10)$$

The dipolar sodium hf coupling tensor $\mathbf{B}^{Na}$ is then a sum of the two tensors $\mathbf{B}_{N-Na}^{Na}$ and $\mathbf{B}_{O-Na}^{Na}$,

$$\tilde{\mathbf{R}}(\alpha,\beta,\gamma)\mathbf{B}^{Na}\mathbf{R}(\alpha,\beta,\gamma) = \mathbf{B}_{N-Na}^{Na}(\rho_{2p\pi}^{N}, r_{N-Na}, \beta_{bond}) + \mathbf{B}_{O-Na}^{Na}(\rho_{2p\pi}^{O}, r_{N-Na}, \beta_{bond}) \quad (11)$$

and depends only on four parameters: the spin densities $\rho_{2p\pi}^{N}$, $\rho_{2p\pi}^{O}$, the N−Na bond length r_{N-Na}, and the bond angle β_{bond}. The Euler matrix **R** transforms the diagonal tensor $\mathbf{B}^{Na}$ into the **g** tensor frame. Taking the experimentally obtained principal values $B_{xx}^{Na} = B_{yy}^{Na} = -1.55$ MHz and $B_{zz}^{Na} = 3.10$ MHz of the ^{23}Na dipolar hf coupling tensor with $\alpha = 90°$, $\beta = 35°$ and the values $\rho_{2p\pi}^{N} = 45.8\%$ and $\rho_{2p\pi}^{O} = 50.2\%$, we determine by a numerical solution of eq 11 $r_{Na-N} = 0.21$ nm and $\beta_{bond} = 142°$. The bond angle of 142° indicates a bent structure of the Na^+-NO adsorption complex (Figure 6) that is typical for a number of nitrosyl complexes.[14,30] The bond length of 0.21 nm is within the range that is known for other nitrosyl complexes[29,30] considering the ionic radius of the Na^+ ion.

Location of the Na^+-NO Complex. Whereas the geometrical and electronic structure of the Na^+-NO complex was derived from the ^{23}Na and ^{14}N hf coupling, information about the sitting and the specific cation adsorption site of the NO molecules can be obtained from the ^{23}Na nq interaction. In the dehydrated NaA zeolite, the 12 sodium ions per unit cell occupy three different cation positions in the large α cages. There are three cations in the plane of the eight-membered rings connecting the α cages but 0.123 nm away from the center (site S5), eight Na^+ cations are located in a trigonal coordination geometry on the symmetry axes of the six-membered rings but 0.02 nm displaced into the α cage (site S2), and the twelfth sodium ion

(28) Hutchinson, C. A., Jr.; McCay, D. B. *J. Phys. Chem.* **1997**, *66*, 3311.

(29) *CRC Handbook of Chemistry and Physics*; Lide, D. R., Ed.; CRC Press: Boca Raton, FL, 1996.

(30) Enemark, J. H.; Feltham, R. D. *Coord. Chem. Rev.* **1974**, *13*, 339.

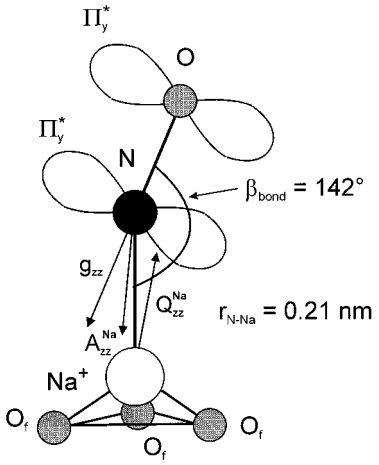

Figure 6. Schematic drawing of the bent structure of the Na^+-NO adsorption complex in zeolite NaA. The *z* principal axes of the **g**, $\mathbf{A}^{Na}$, and $\mathbf{Q}^{Na}$ tensors lie within the Na−N−O complex plane and form an angle with the Na^+-NO bond direction of 38°, 3°, and 8°, respectively. The unpaired electron is localized mainly in the antibonding $^2\Pi_y^*$ molecular orbital of the NO molecule, which is also within the complex plane. The cation at site S2 is coordinated to the framework oxygens, O_f, in the six-membered rings in a trigonal symmetry. Only the three oxygens in the first coordination sphere are shown.

is found in front of a four-membered ring (site S3).[31] ^{23}Na nutation NMR spectroscopy[32] of dehydrated NaA showed that the Na^+ cations at site S2 have a nq coupling constant $e^2qQ/h = 5.8$ MHz, with an asymmetry parameter $\eta = 0$ corresponding to $Q_{xx} = Q_{yy} = -0.48$ MHz and $Q_{zz} = 0.96$ MHz. The *z* axis of the nq tensor points along the trigonal symmetry axis of this cation site. For sodium ions at sites S3 and S5, smaller nq couplings $e^2qQ/h = 3.2$ MHz with a larger asymmetry parameter $\eta = 0.9$ ($Q_{xx} = -0.51$ MHz, $Q_{yy} = -0.03$ MHz, $Q_{zz} = 0.54$ MHz) have been found.[32]

The determined principal values of the sodium nq interaction tensor $|Q_{xx}^{Na}| = 0.41$ MHz, $|Q_{yy}^{Na}| \leq 0.23$ MHz, and $|Q_{zz}^{Na}| \leq 0.64$ MHz in the Na^+-NO adsorption complex are in the range of those nq parameters. The *y* and *z* principal axes of $\mathbf{Q}^{Na}$ are in the Na−NO plane, where the mean orientation of the *z* axis deviates by only 8° from the Na^+-NO bond direction (Figure 6). It is reasonable to assume that for the bent structure of the Na^+-NO complex, the principal values Q_{yy}^{Na} and Q_{zz}^{Na} of the sodium nq tensor lying within the complex plane are more affected by the complexation of the Na^+ cation with NO than the Q_{xx}^{Na} principal value. Hence, we may expect changes in Q_{yy}^{Na} and Q_{zz}^{Na} upon formation of the adsorption complex. The observed distribution in the magnitude and orientation of Q_{yy}^{Na} and Q_{zz}^{Na} might indicate some variance in the individual bond angles β_{bond} of the Na^+-NO complex. In contrast, Q_{xx}^{Na} does not show a significant variance, and its value is close to that of uncoordinated sodium cations located at the six-membered rings (site S2). For formation of the adsorption complex at this cation position, no variance in Q_{xx}^{Na} is expected because of the axial symmetry of the nq tensor of the uncoordinated sodium ions.[32] The *x* axis of the nq tensor of the sodium ion is always directed perpendicular to the complex plane (Figure 4) and hence also perpendicular to the trigonal symmetry axis of the cation site at the six-membered rings. Then, in the case of an axially symmetric nq tensor of the uncoordinated cation, the value of Q_{xx}^{Na} should be independent of different azimuthal orientations of the complex plane about the trigonal symmetry axis, a disorder very likely for such weakly bound adsorption complexes. This is obviously not the case for the orthorhombic nq tensors of the uncoordinated Na^+ ions at sites S3 and S5. Therefore, we may conclude that the Na^+-NO complex in zeolite NaA is preferably formed at sodium cations at site S2 located near the six-membered rings.

6. Conclusions

The combination of orientation-selective pulsed ENDOR spectroscopy at W- and X-bands is a very useful tool for the determination of hf and nq coupling tensors of ligand nuclei in paramagnetic complexes in cases where the ESR powder pattern is governed by anisotropic electron Zeeman and hf interactions. The results gave direct evidence that nitric oxide is actually adsorbed at sodium cations in zeolite NaA at low temperatures. The determination of the ^{23}Na and ^{14}N hf coupling tensors together with the ^{23}Na nq interaction tensor allows a detailed characterization of the formed Na^+-NO adsorption complexes. From the hf couplings we obtain the geometrical and electronic structure of the complex. The sodium nq interaction provides insight into at which specific cation site the NO molecules are adsorbed. The Na^+-NO adsorption complexes have a bent complex structure with a Na−NO bond length of 0.21 nm. NO adsorption complexes are most likely formed with sodium cations at the six-membered rings. Upon complex formation, the electron pair acceptor property of the Na^+ ion gives rise to a shift of the NO electron density toward the nitrogen atom, $Na^+-:\ddot{N}^- = O:^+$. The shift of the electron spin density is probed via the dipolar nitrogen hf interaction, thus offering an alternative way to directly measure the acidity of Lewis acid sites in zeolites by NO probe molecules.

Acknowledgment. This research was supported by the Deutsche Forschungsgemeinschaft within the Sonderforschungsbereich 294 and the Schwerpunktprogramm "Hochfeld EPR-Spektroskopie". The authors thank R. Böttcher and D. Michel, Universität Leipzig, for helpful discussions, and A. Gutsze, Medical School Bydgoszcz, for providing the NaA zeolite.

JA001888U

(31) Pluth, J. J.; Smith, J. V. *J. Am. Chem. Soc.* **1980**, *102*, 4704.
(32) Tijink, G. A. H.; Janssen, R.; Veeman, W. S. *J. Am. Chem. Soc.* **1987**, *109*, 7301.